SSRG International Journal of Mechanical Engineering
ISSN: 2348-8360/ https://doi.org/10.14445/23488360/IJME-V12I9P107

Volume 12 Issue 9, 65-77, September 2025

Original Article

Vibration Characteristics of Blade Adjustment Gear Train for 8MW Class Offshore Wind Turbines

Min-Woo Kim[1], Yu-Jin Jeong[1], Hyoung-Woo Lee[2]

[1]*Department of Convergence Engineering, Jungwon University, Republic of Korea.*
[2]*Department of Aero Mechanical Engineering, Jungwon University, Republic of Korea.*

[2]*Corresponding Author : leehwoo@jwu.ac.kr*

Received: 08 July 2025 Revised: 09 August 2025 Accepted: 10 September 2025 Published: 30 September 2025

Abstract *- This paper reports on a study of the vibration characteristics of the blade adjustment gear train for 8MW class offshore wind turbines. A method for analyzing the vibrations of the blade adjustment gear train was proposed by combining the rotational vibration model of the planetary gear train with the finite element models of the housing and carrier using the sub-structuring method. Applying 10%, 20%, …, 100% of the largest LDD load showed that both bearing stiffness and the primary natural frequency increase with higher LDD loads. Furthermore, the primary natural frequency for the highest load in the LDD data was found to be 104.26 Hz, which exceeds the operating speed of 84.87 rpm (5.09 Hz), indicating that vibrations due to LDD load variations do not occur within the operating speed range. In addition, analysis of critical speeds for the blade adjustment gear train showed that critical speeds related to mass unbalance, gear mesh frequency, and bearing defects do not occur within the operating speed range (84.87 rpm). Also, by utilizing AGMA 6000-B96, an acceptable displacement for vibration was selected, and the displacement occurring under LDD load conditions was compared with the acceptable displacement to assess vibration safety. The response analysis results for the planetary gears and output shaft bearings at the 1st, 2nd, and 3rd stages all satisfied the acceptable levels. This work shows that vibration problems in complex gear systems can be accurately predicted during the simulation phase. This can dramatically reduce development cost and time by detecting and correcting design defects before expensive prototyping or real-world testing. In the future, we plan to verify the reliability of the model by comparing it with the theoretical analysis results through real-world experiments.*

Keywords *- Wind turbine, Vibration, Transmission Error, Response Analysis.*

1. Introduction

Among the components of a wind turbine, the pitch system maintains the appropriate power output by measuring the electrical output through an electrical control device. If the output exceeds or falls below the optimal level, the system sends a signal to the blade control device to adjust the angles of the blades, thus ensuring the maintenance of the correct output. Through the adjustment of blade angles, the pitch system also facilitates functions such as starting operation to gain sufficient starting torque when the wind speed exceeds the startup threshold, maintaining constant rated output above the rated wind speed, and stopping during high or low wind speeds. The blade adjustment gear train plays a role in rotating the blades for output control in the wind turbine. The wind turbine blade adjustment gear train is composed of a planetary gear system, shafts, and bearings.

Research on the safety evaluation of the gear system, including the analysis of its natural frequency and dynamic response, has been ongoing. J.W. David and L.D. Mitchell expressed the dynamic behavior of geared rotor systems through motion equations and claimed that the dynamic coupling terms in these systems cannot be neglected [1, 2]. Takuzo Iwatsubo et al. considered the dynamic coupling term of lateral-torsional vibrations in spur gears to analyze the response to mass unbalance and changes in gear stiffness. Hiroshi IIDA et al. argued that the response of a gear system model that includes the dynamic coupling term of torsional-flexural vibration in spur gears differs from models that do not consider this term. Additionally, P. Schwibinger and R. Nordmann demonstrated that the dynamic coupling term of torsional and lateral vibrations in spur gears affects the stability of the gear system [3-6]. H. Ahmet Kahraman et al. analyzed the critical speed of M. A. Prohl, J. W. Lund, and P. N. Bansal et al. or A. Kahraman or J. S. Kim et al. created a single-stage spur gear system by considering the dynamic coupling term of torsional and tranverse vibrations and using the finite element method to determine the response to mass unbalance and tooth machining errors.

F. K. Choy developed a dynamic model for a three-stage spur gear system considering the dynamic coupling term, and

analyzed the steady-state and transient responses and the structural vibrations of the gear system housing transmitted through bearings [7-9]. The vibration analysis methods for geared rotor systems include the transfer matrix and finite element methods. M. A. Prohl, J. W. Lund, and P. N. Bansal et al. presented models and boundary condition application methods for rotor systems using the transfer matrix method, and analyzed the natural characteristics, dynamic response, and critical speeds of rotor systems supported by bearings. A. Kahraman introduced a three-dimensional dynamic model of a planetary gear system composed of helical gears, and analyzed its natural modes and forced vibration response. J. S. Kim et al. created a transfer matrix model for a planetary gear system, analyzing its natural frequency and forced vibrations. Robert G. Parker et al. developed a finite element model for a planetary gear system and analyzed its natural frequency, vibration modes, and dynamic responses [10-12]. Mengyan Nie, and Ling Wang were conducted fault diagnosis on wind turbines and analyzed the vibrations of the gear train [13]. Smolders et al. performed vibration modeling of the drivetrain and analyzed its natural frequencies [14]. Tchakoua, P. et al. discussed vibration analysis and predictive diagnostic techniques for planetary gear systems [20].

The aforementioned studies conducted vibration analyses only on the gear train, without finite element modeling of the housing and carriers. Therefore, a vibration analysis that includes both the finite element models of the housing, carriers, and the planetary gear train is needed.

This study examined the vibration characteristics of a blade adjustment gear train for an 8MW class offshore wind turbine. The proposed method analyzes the vibrations of the blade adjustment gear train by combining the rotating body vibration model of the planetary gear train with the finite element models of the housing and carriers using substructure synthesis. After modeling the vibration excitation sources acting on the blade adjustment gear train, such as mass unbalance, gear mesh frequency, and bearing defect errors, critical speed analysis was conducted to determine if resonance occurs within the operating speed range. Additionally, vibration characteristics were analyzed by identifying changes in bearing stiffness and the primary natural frequency when applying 10%, 20%, …, 100% of the largest value from the Load Duration Distribution (LDD) load. The stiffness of the bearing is calculated by the deflection in axial and radial directions. Load conditions are included in deriving each deflection, and the load data of the wind power generator continuously changes the load over time. In the case of a rotating structure, the stiffness of the rolling bearing changes with the load [18, 19]. Existing gearbox research performed free vibration analysis (mode analysis) with rigidity input for a fixed load. However, since the gearbox for wind turbines has numerous LDD data and the bearing stiffness changes with each load, an analysis that takes this into account should be performed. Furthermore, the excitation forces caused by transmission errors in the 1st to 3rd stage planetary gear system were modeled. To perform a safety evaluation of the vibration displacement in the wind turbine blade adjustment gear train, AGMA 6000-B96 was utilized to select an acceptable vibration displacement, and the displacement occurring under LDD load conditions was compared with this acceptable displacement to assess vibration safety.

2. Vibration Modeling and Vibration Characteristic Analysis of the Blade Adjustment Gear Train

2.1. Vibration Modeling of the Blade Adjustment Gear Train

The vibration model of the blade adjustment gear train was designed using MASTA 13.0.1, a commercial gear analysis software. Figure 1 illustrates the power flow of the blade adjustment gear train. The blade adjustment gear train consists of a three-stage planetary gear system where the power from the motor, entered through the 1st sun gear, is transmitted to the output shaft via the 2nd and 3rd-stage planetary gear systems. In the blade adjustment gear train, with the ring gear fixed, the output shaft of each stage is connected to the subsequent input shaft via splines. In the three-stage planetary gear system of the blade adjustment gear train, the 1st and 2nd stages consist of three planetary gears each, and the 3rd stage consists of four planetary gears. The number of teeth on the sun gear, planetary gears, and ring gear in the 1st stage are 16, 47, and 110, respectively; in the second stage, they are 16, 25, and 68; and in the 3rd stage, they are 20, 23, and 68. The reduction ratios are 7.875 for the first stage, 5.25 for the 2nd stage, and 4.4 for the 3rd stage, with an overall reduction ratio of about 180.57. The rotational speed of the motor entering through the 1st sun gear is approximately 84.871 rpm, which is reduced through the gearbox to 0.47 rpm.

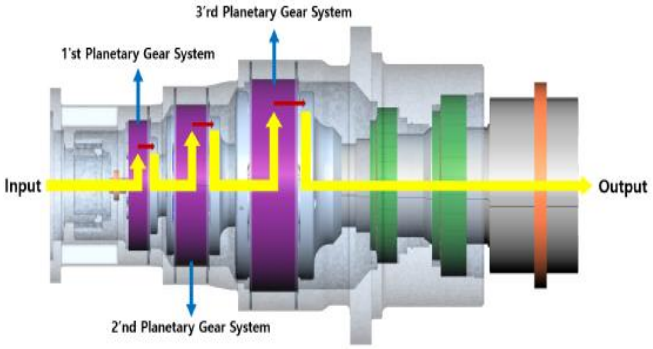

Fig. 1 Blade adjustment gear train power flow

Table 1 shows the specifications for the 1st-stage planetary gear system of the blade adjustment gear train, while respectively show the specifications for the 2nd and 3rd-stage planetary gear systems of the blade adjustment gear train.

Table 1. Blade adjustment gear train planetary information

Stage	1			2			3		
	Sun	Planetary	Ring	Sun	Planetary	Ring	Sun	Planetary	Ring
Planetary Gear	3			3			4		
Module	1.75			3.5			4.5		
Pressure Angle	27°			27°			27°		
Number of Teeth	16	47	110	16	25	68	20	23	68
Center Distance	55.5			74			99.7		
Reduction Ratio	7.875			5.25			4.4		

2.2. Vibration Modeling of the Blade Adjustment Gear Train

Generally, finite element methods are used for structural analysis; however, the time taken to divide the mesh and the computational effort required are significant issues for large structures. To address these issues, the substructuring method divides the entire structure into several elements, independently calculates modal parameters for each element, and then combines the elements using geometric compatibility conditions as constraints. The modal parameters, stresses, and strains of the desired structure can thus be obtained [15].

Using MASTA 13.0.1, the gear train of a pitch reducer is modeled as a rotating body vibration, and the housing and carriers are connected using the substructuring method with the ANSYS 2023R2 finite element model. Figure 2 displays the finite element model of the housing created using ANSYS 2023R2.

Figure 3 illustrates the connection points between the gear train and the housing. The output shaft bearing of the gear train contacts the Output Housing, and the ring gear sections of each stage are connected to the corresponding ring gear sections of the housing.

Fig. 2 Housing finite element model

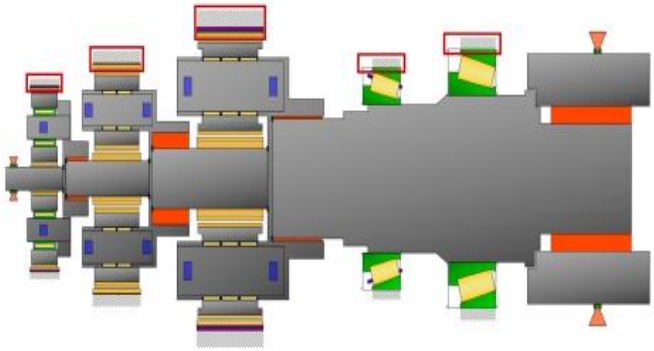

(a) Gear train connection

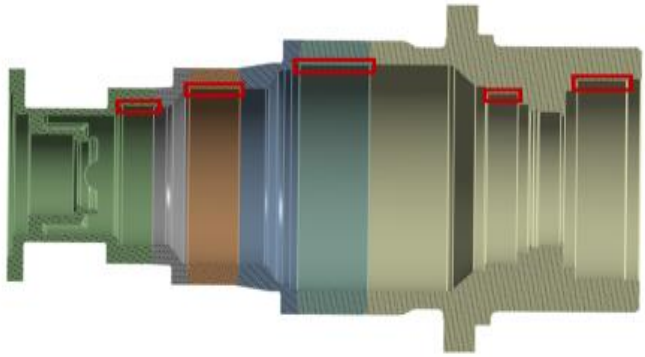

(b) Housing connection

Fig. 3 Housing and gear train connection

Figure 4 shows the finite element model of the carriers prepared for synthesis with the gear train model. The 1st carrier's finite element model consists of 561,214 nodes and 393,420 elements, the 2nd carrier's consists of 680,979 nodes and 470,645 elements, and the 3rd carrier consists of 114,482 nodes and 73,528 elements.

Figure 5 illustrates the connection points between the gear train and the carriers. The substructuring of the carriers involves connecting the nodes at the points where a carrier contacts the planetary pin and connecting the nodes at the spline section where a carrier connects to the next stage.

Fig. 4 Carrier finite element model

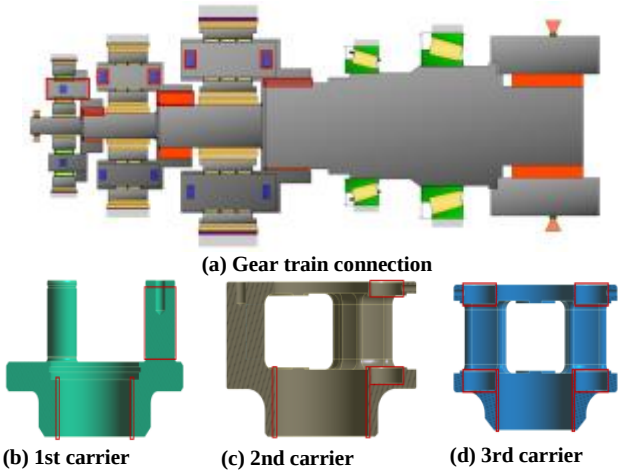

(a) Gear train connection

(b) 1st carrier (c) 2nd carrier (d) 3rd carrier

Fig. 5 Carrier and gear train

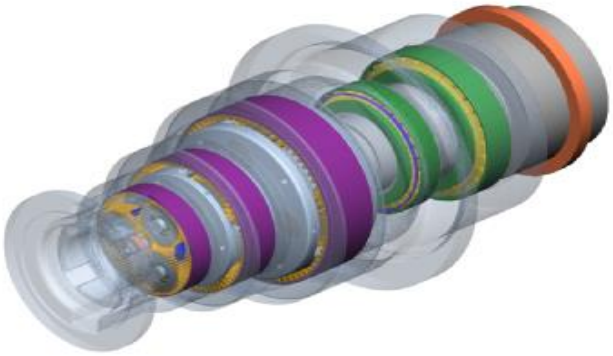

Fig. 6 Vibration model

Figure 6 shows the vibration model that combines the finite element models of the housing and carriers with the planetary gear train using the substructuring method.

2.3. Analysis of Natural Frequency Characteristics with LDD Load Variation

The vibration system of the wind turbine blade adjustment gear train can be expressed as shown in Equation (1).

$$[M]\ddot{q} + [K]q = 0 \quad (1)$$

$[M]$ is the system mass matrix, $[K]$ is the system stiffness matrix, and q is the degree of freedom of the system [18]. Typical industrial reducers operate under constant, unvarying loads. However, wind turbines must undergo vibration analysis for various LDD loads. The stiffness of the rolling bearings in the wind turbine blade adjustment gear train changes according to the torque applied; therefore, it is essential to study the impact of LDD load variations on the primary natural frequency.

The stiffness of the bearing is calculated by the deflection in axial and radial directions. Load conditions are included in deriving each deflection, and the load data of the wind power generator continuously changes over time. In the case of a rotating structure, the stiffness of the rolling bearing changes with the load [19, 20]. Existing gearbox research performed free vibration analysis(mode analysis) with rigidity input for a fixed load.

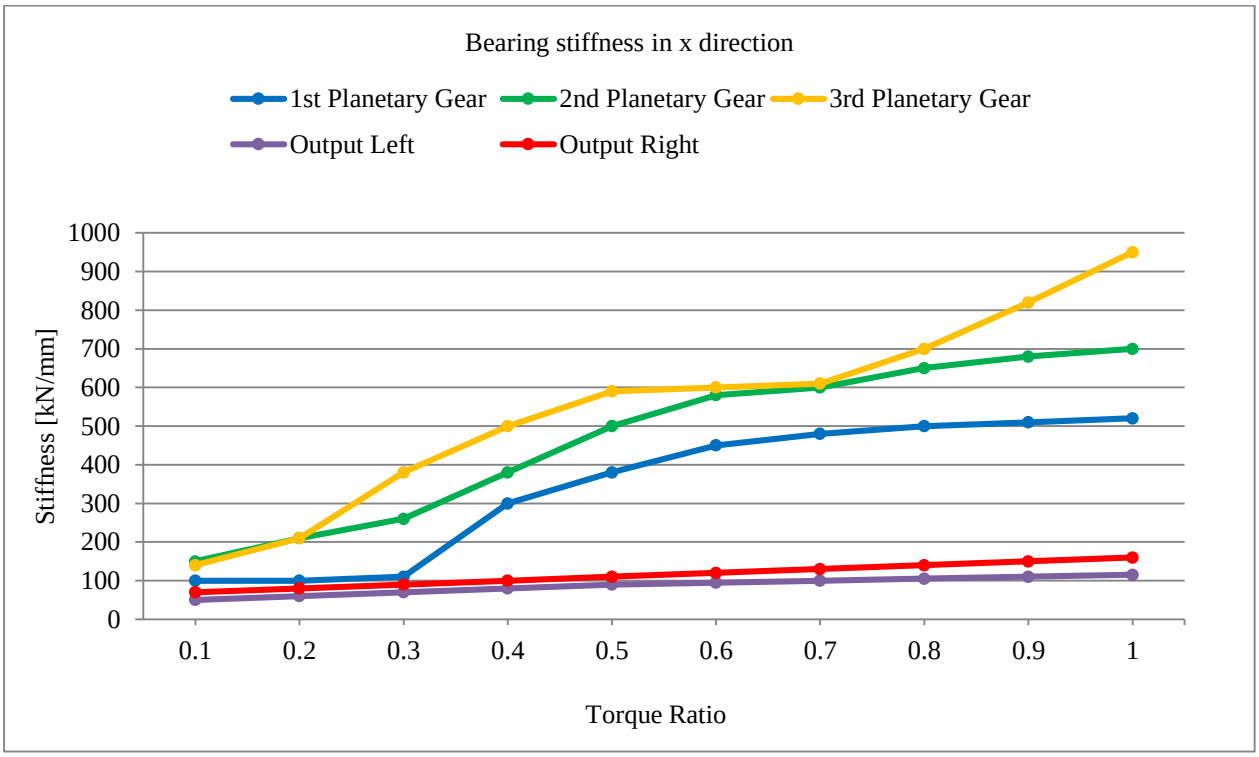

Fig. 7 Variation of bearing stiffness in the x-direction according to load

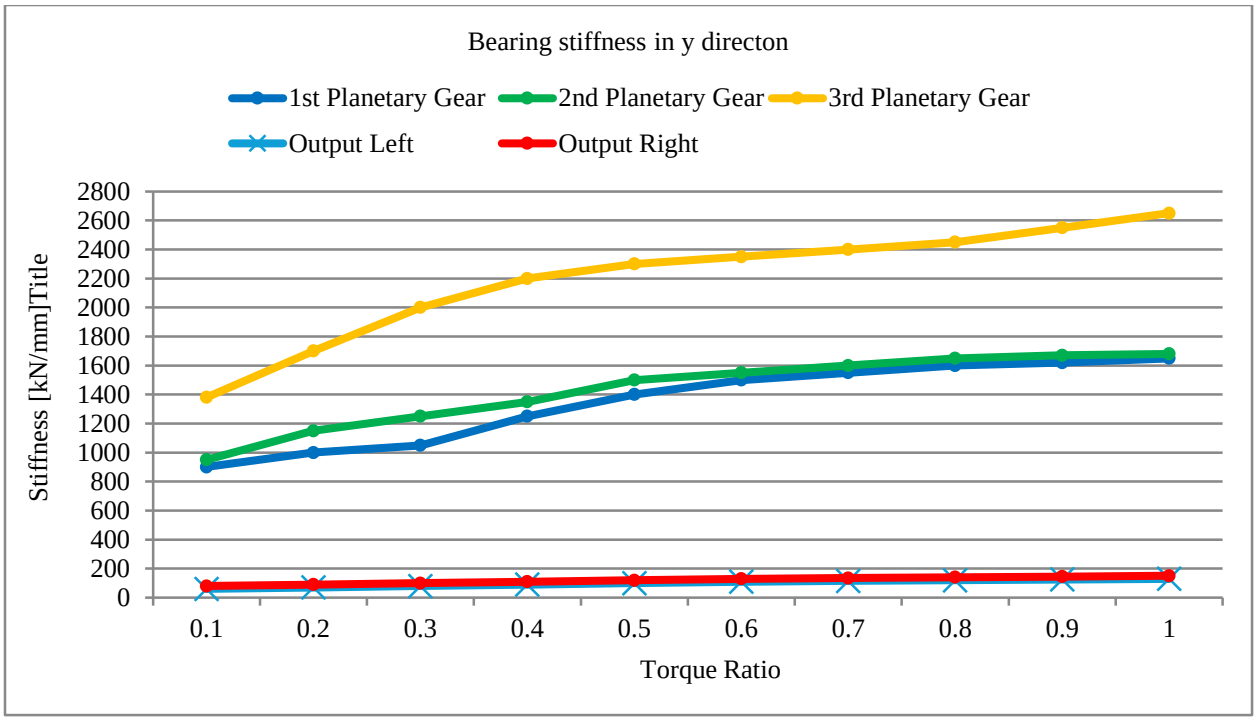

Fig. 8 Variation of bearing stiffness in the y-direction according to load

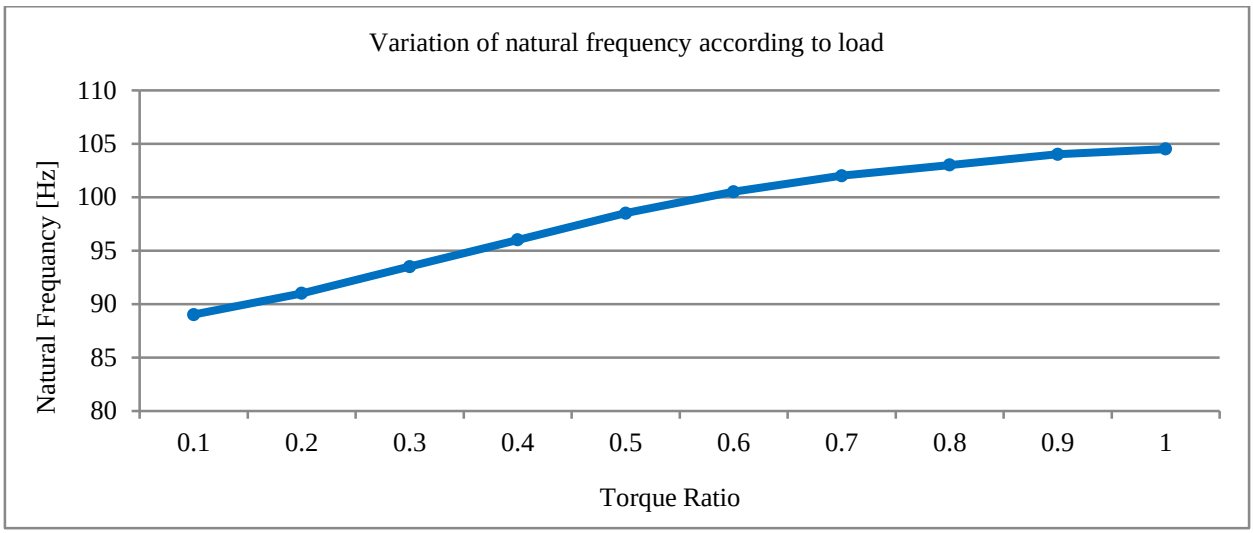

Fig. 9 Variation of natural frequency according to load

However, since the gearbox for wind turbines has numerous LDD data and the bearing stiffness changes with each load, an analysis that takes this into account should be performed. Due to insufficient research on the changes in natural frequency characteristics in response to LDD load variations, this study conducted research on the natural frequency of the blade adjustment gear train in response to changes in LDD loads.

Figures 7 to 8 show the changes in natural frequency according to bearing stiffness, taking the largest load in LDD as 1 and applying 10%, 20%, …, 100% of this largest load.

Figure 7 illustrates the changes in stiffness in the x-direction of the bearings for each stage due to load changes. It was observed that there is a significant change in stiffness in the x-direction with load variation. Figure 8 shows the changes in stiffness in the y-direction of the bearings for each stage according to load changes. A significant change in stiffness in the y-direction was noted with load variation. Figure 9 displays the changes in the primary natural frequency due to load variations. Since the lowest primary natural frequency is 81.47 Hz, which exceeds the operating speed of 84.87 rpm (5.09 Hz), it can be concluded that all LDD data are safe within the operating speed range.

Table 2 shows the natural frequency of the vibration model, which combines the finite element model of the housing and carriers with the planetary gear train using the substructuring method, under the condition of the smallest torque among the LDD data.

Table 2. Natural frequency

Mode	Natural Frequency [Hz]
1	104.26
2	118.79
3	193.86
4	209.87
5	290.42
6	323.55

3. Excitation Source Modelling and Critical Speed Analysis of the Blade Adjustment Gear Train

3.1. Vibration Excitation Source Modeling

The excitation sources acting on the blade adjustment gear train include excitation due to mass unbalance, gear mesh frequency, and excitation due to bearing and installation errors. The primary causes of gear mesh frequency are manufacturing errors in the gear teeth and system deformations due to load, which are expressed as the product of the rotational speed and the number of gear teeth.

Mass imbalance refers to the eccentric mass present due to manufacturing errors, which corresponds to the rotational speed. The excitation frequencies caused by defects in rolling bearings include Fundamental Train Frequency (FTF), Ball Spin Frequency (BS), Outer Racer Frequency (OR), and Inner Racer Frequency (IR) [14].

Table 3 presents the excitation frequency ratios considering the mass unbalance and gear mesh frequency of the blade adjustment gear train, where 1X indicates the changes in rotational speed entering the 1st-stage sun gear. The characteristics of the bearings for each stage are shown in Table 4, and the excitation sources caused by bearing defects are listed in Table 5.

Table 3. Excitation frequency of mass unbalance and gear mesh frequency

Excitation Source	Excitation Frequency Ratio		
		Sun	Planetary
Mass Unbalance	Stage 1	1X	0.127X
	Stage 2	0.127X	0.024X
	Stage 3	0.024X	0.005X
Gear Mesh Frequency	Stage 1	16X	
	Stage 2	2.03X	
	Stage 3	0.48X	

Table 4. Rolling bearing information

Stage	1	2	3	Output Left	Output Right
Number of Balls	16	20	29	31	29
Pitch Diameter [mm]	34	38.5	59	200.328	230.271
Ball Diameter [mm]	4	3.5	4	20.1	25.1
Contact Angle [°]	0	0	0	17	15.75

Table 5. Excitation frequency ratio of the bearing

Stage	1	2	3	Output Left	Output Right
FTF	0.08X	0.02X	0.004X	0.004X	0.004X
BS	0.75X	0.19X	0.06X	0.04X	0.04X
OR	1.27X	0.31X	0.11X	0.12X	0.13X
IR	1.6X	0.37X	0.12X	0.12X	0.1X
rps	0.18	0.03	0.008	0.008	0.008

3.2. Critical Speed Analysis

Vibration and noise of the wind turbine blade adjustment gear train occur when the excitation frequency of the blade adjustment gear train matches its natural frequency. Let the excitation frequencies be denoted as $\gamma_i, i = 1,2,3 \dots N$, and the natural frequencies of the pitch reducer as λ_i. If $i = 1,2,3 \dots N$, resonance occurs when $\gamma_i = \lambda_i$. If the excitation frequency is set as $\gamma_i = c_i\omega_{cr}$, the critical speed ω_{cr} becomes $\omega_{cr} = \lambda_i/c_i$. Here, c_i is the coefficient of the excitation frequency.

The input speed of the blade adjustment gear train is 84.87 rpm; the changes in excitation sources according to variations in input speed are shown in Tables 5 and 7. The natural frequency is calculated by considering the finite element models of the housing and carriers and the planetary gear train under the condition of the highest torque among the LDD data. Figure 10 presents the Campbell Diagram for mass unbalance.

Figure 11 shows the Campbell Diagram for gear mesh frequency. Figure 12 illustrates the Campbell Diagram for bearing defects (FTF, BS, OR, IR). From Figures 10 to 12, it can be seen that there are no critical speeds related to mass unbalance, gear mesh frequency, or bearing defects within the operating speed range.

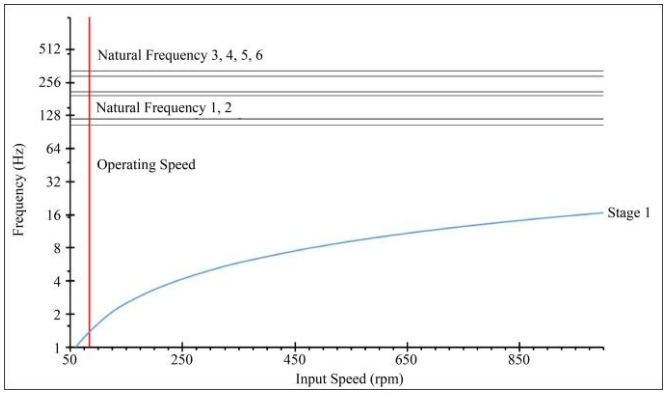

Fig. 10 Campbell diagram of mass unbalance

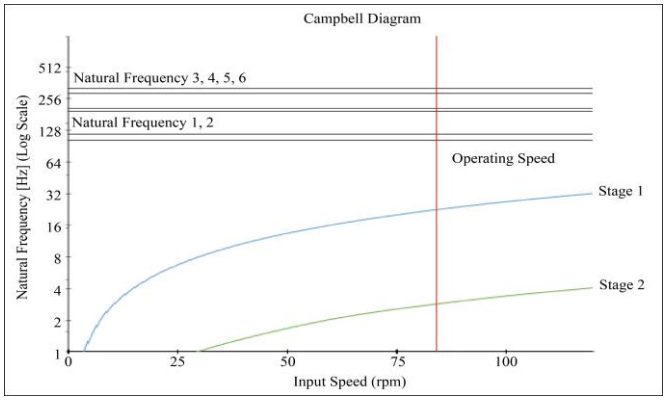

Fig. 11 Campbell diagram of gear mesh frequency

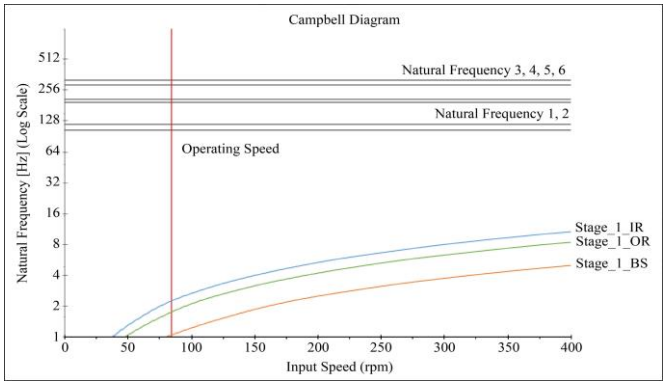

(a) Stage 1

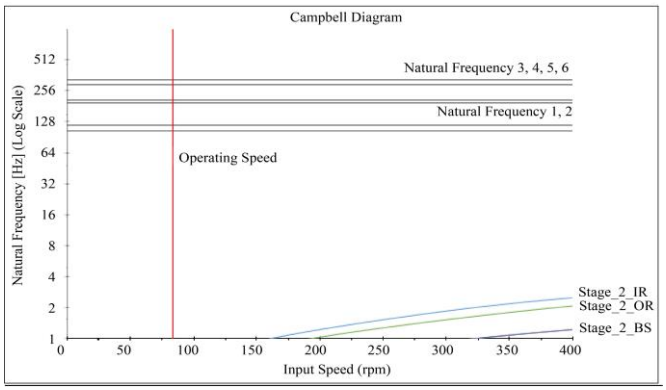

(b) Stage 2

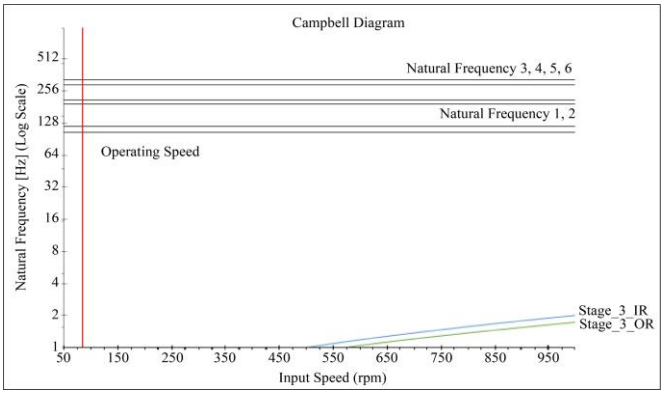

(c) Stage 3

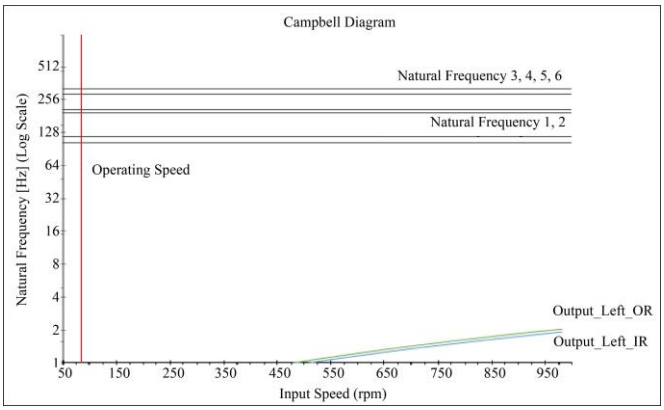

(d) Output left

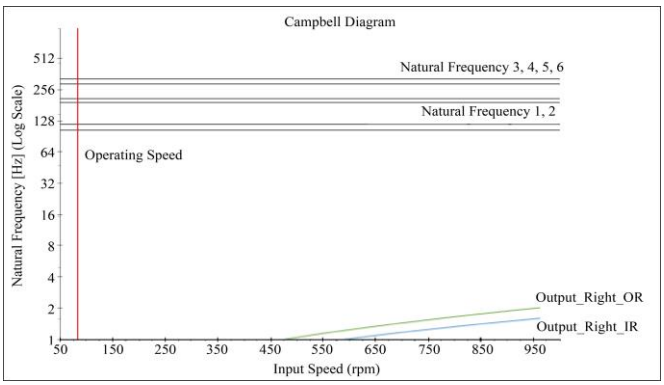

(e) Output light

Fig. 12 Campbell diagram of bearing

4. Analysis of the Dynamic Characteristics of the Blade Adjustment Gear Train

4.1. Excitation Modeling

When a load is applied to a gear, noise occurs due to tooth collisions caused by transmission errors. Therefore, to examine the characteristics of transmission errors, it is necessary to model the excitation sources of transmission errors. Table 6 shows the causes and occurrence factors of transmission errors. Transmission errors are caused by installation errors such as shaft misalignment and gear eccentricity, as well as manufacturing errors and elastic deformation due to transmitted force. For wind turbines,

elastic deformation due to transmitted force is a more significant cause than installation and manufacturing errors [6]. To determine the amount of tooth deformation when gears are engaged, it is necessary to calculate the tooth stiffness. If tooth stiffness is expressed as a function of time, it becomes a periodic function with gear mesh frequency as the fundamental frequency. Since a periodic function can be transformed into a Fourier series, tooth stiffness, denoted as $K(t)$, can be calculated using the following Equation (2).

$$K(t) = K_o + \sum_{i=1}^{N}[K_{ic}\cos(i\Omega t) + K_{is}\sin(i\Omega t)] \quad (2)$$

Here, K_o is the average tooth stiffness, K_{ic}, K_{is} are the coefficients of the Fourier series, N is the number of partial sums of the Fourier series, and t is time. Table 7 shows the primary harmonic component considering the average value of tooth stiffness. As with all mechanical elements, the gear tooth profile cannot be a perfect involute curve. Geometric errors generated during manufacturing or installation can change the speed ratio of gear pairs, and such dynamic changes are observed to be the main cause of high-frequency vibrations in the gear system due to dynamic contact forces at the gear contact area [15]. Therefore, accurate measurement or theoretical analysis of these gear errors directly impacts the vibration analysis of the system. Research on gear errors has shown that gear errors vary similarly to a periodic function, with the gear mesh frequency as the fundamental frequency. It also includes factors that cause an unusual frequency response known as the "Ghost Frequency" [16]. The ghost frequency is a unique frequency caused by the errors in the tooth profile curves of the gear cutting tool used in the gear manufacturing process. Therefore, gear errors can be expressed mathematically as follows:

$$e(t) = \sum_{i=1}^{N}[e_{ic}cos(i\Omega t) + e_{is}sin(i\Omega t)] + e_{gc}cos(\Omega_g t) + e_{gs}sin(\Omega_g t) \quad (3)$$

Here, Ω_g represents the ghost frequency. Each gear in a gear pair acts as an independent rotor, and the centrifugal force caused by the eccentricity of the center of mass induces vibrations in the gear system. Figures 13 to 15 show the transmission error at different gear contact positions according to Equation (3).

Table 6. Occurrence factor and causes of transmission error

Occurrence Factor	Causes
Gear tooth deflection	Transmitted force Elastic deformation
Shaft deflection	
Gear tooth profile error	Manufacturing error
Gear pitch error	
Gear eccentricity	Installation error
Gear wobble	
Shaft misalignment	

Table 7. Transmission error 1st harmonic

Stage	Meshing	1st harmonic(μm)
1st	sun - planet	1.284
	planet - ring	0.4974
2nd	sun - planet	2.6066
	planet - ring	2.2335
3rd	sun - planet	3.903
	planet - ring	3.9332

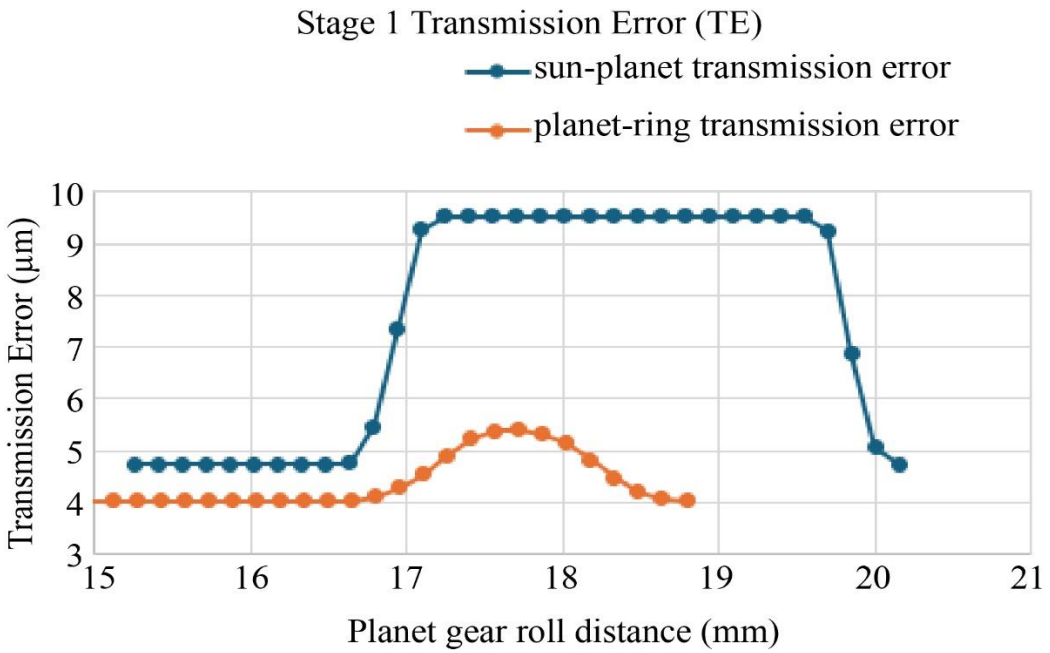

Fig. 13 Stage 1 transmission error

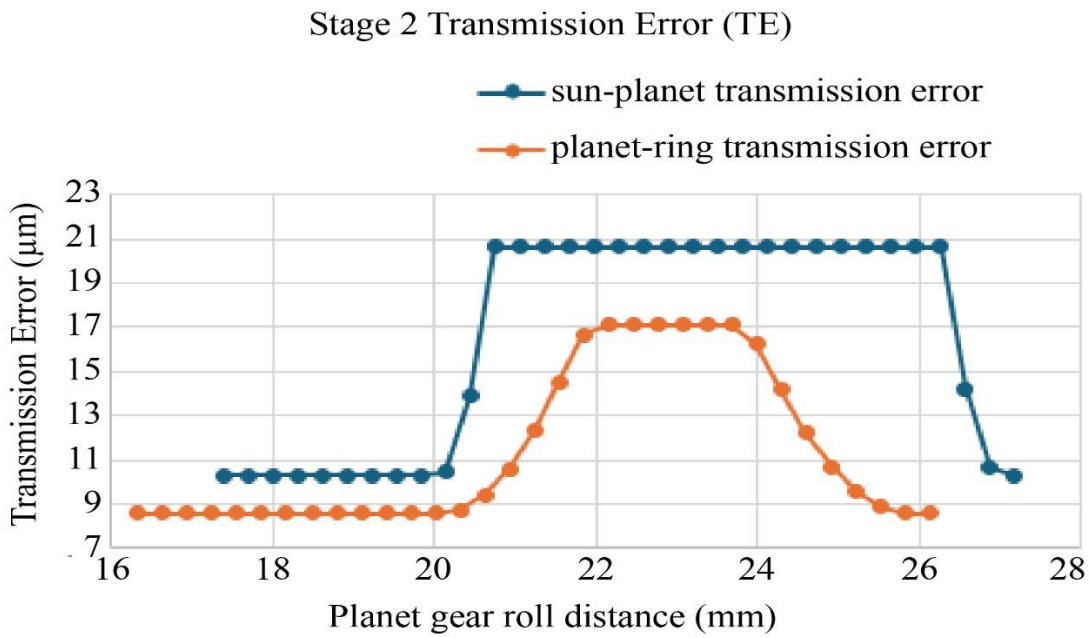

Fig. 14 Stage 2 transmission error

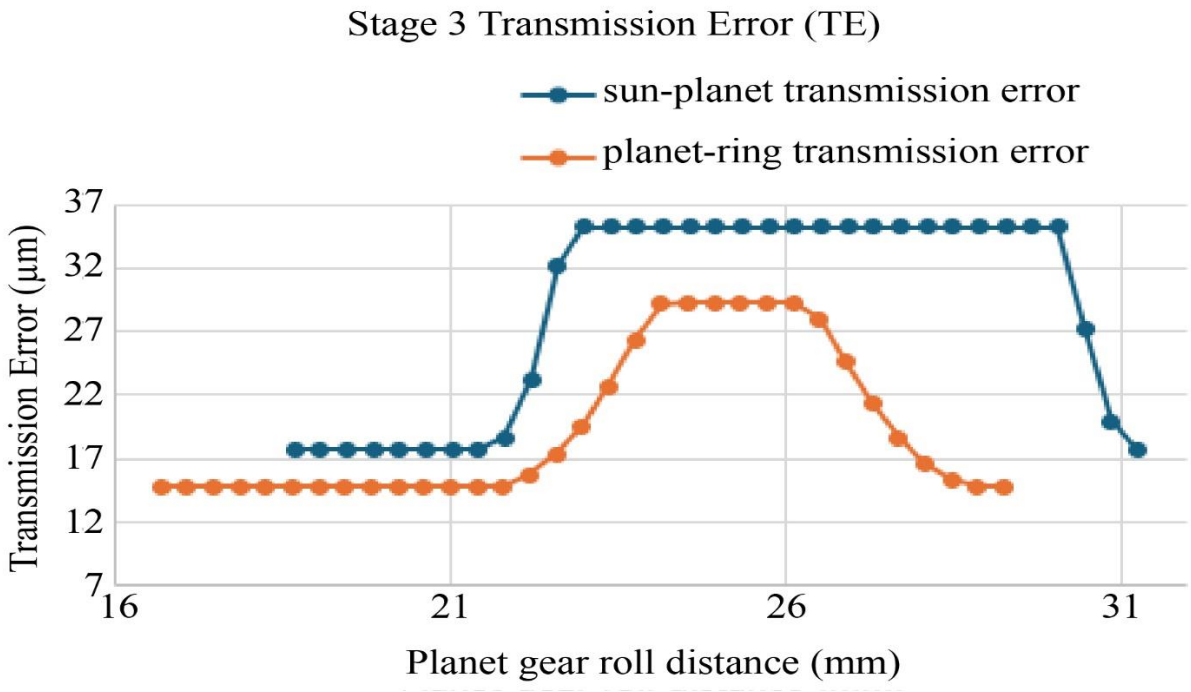

Fig. 15 Stage 3 transmission error

4.2. Response Analysis

The Gear Rotor System experiences vibrations due to excitation sources such as mass unbalance and gear mesh frequency. Vibrations in the geared rotor system can lead to a shortened lifespan. The wind turbine blade adjustment gear train is a functional component that is expected to last for more than 20 years. Therefore, it is necessary to perform a safety assessment for displacements caused by vibrations. In this study, to perform a safety assessment on the vibration displacement of the wind turbine blade adjustment gear train, the American Gear Manufacturers Association (AGMA) standard AGMA 6000-B96 was used to select an acceptable displacement. The displacement that occurs under extreme load conditions was compared with the acceptable displacement to assess the vibration safety [17].

Figure 16 presents a graph of the acceptable displacement according to the AGMA 6000-B96 standard. The x-axis of the graph represents the reference frequency for calculating the tolerance, and the y-axis represents the acceptable displacement. Classes A and B on the graph classify gears based on their Pitch Line Velocity (PLV).

Table 9 shows the pitch line velocity and reference frequency used for selecting the acceptable displacement. The pitch line velocity is that of the sun gear in the planetary gear system, and the rotational speed of the gears can be calculated from the input speed of the 1st-stage sun gear using the reduction ratios of each stage and Equation (4). In Equation (4), N is the rotational speed of the gear (rpm), and D_p is the pitch diameter.

$$PLV = \frac{\pi N D_p}{60.000}[m/s] \quad (4)$$

In Figure 16, the pitch line velocities for the 1st, 2nd, and 3rd stages are all below 25.4 m/s, classifying them as Class A. The acceptable displacement was determined at the point where the reference frequency line intersects with the Class A line on the Y-axis. The acceptable displacements calculated through reference frequency and pitch line velocity are shown in Table 11. In Table 11, the acceptable level for the 1st-stage planetary gear system is 67μm, for the 2nd-stage planetary gear system is 86μm, and for the 3rd-stage planetary gear system is 400μm.

Figure 17 illustrates the displacement measurement locations for the planetary gears and the output shaft bearings. The positions of the planetary gears are represented by phase angles corresponding to the number of planetary gears. The 1st and 2nd stages, which consist of three planetary gears, are represented at 0°, 120°, and 240°, respectively, while the 3rd stage, consisting of four planetary gears, is represented at 0°, 90°, 180°, and 270°. The bearings on the output shaft are distinguished as Bearing A for the front bearing and B for the rear bearing.

Tables 10 to 13 show the response results for the planetary gears and output shaft bearings at the 1st, 2nd, and 3rd stages. From the response analysis, among the 1st-stage planetary gears, the x-direction displacement of the planetary gear located at phase angle 0° was approximately 50.336μm, which satisfies the acceptable displacement of 65μm. Among the 2nd-stage planetary gears, the y-direction displacement of the planetary gear located at phase angle 240° was approximately 16.723μm, which is safe as it is within the acceptable displacement of 86μm. For the 3ird stage, the displacements in the x or y directions of all planetary gears were approximately 11 to 12μm, satisfying the acceptable displacement of 400μm. For the output shaft bearings, the x-direction displacement of Bearing A was 7.844μm, and the y-direction displacement of Bearing B was 5.296μm, both satisfying the acceptable displacement of 400μm.

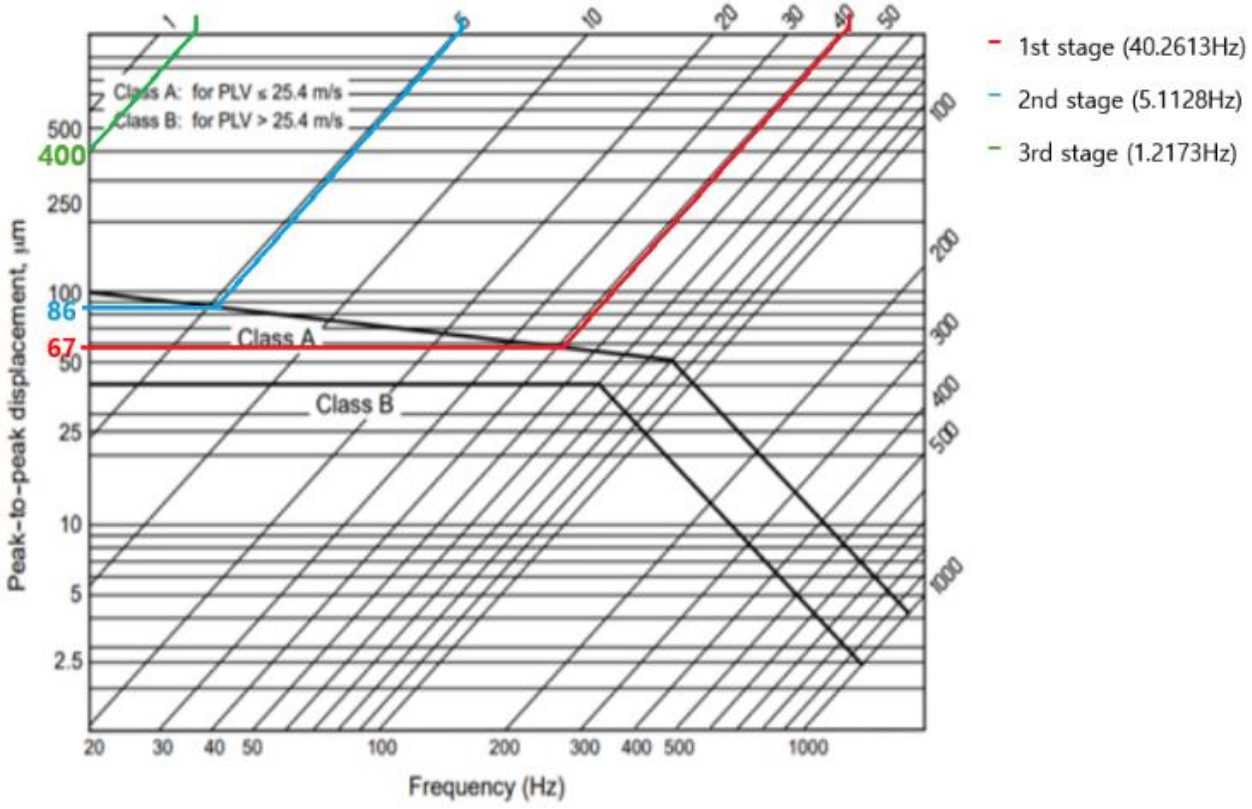

Fig. 16 Selection of displacement tolerance using AGMA 6000-B96 specification

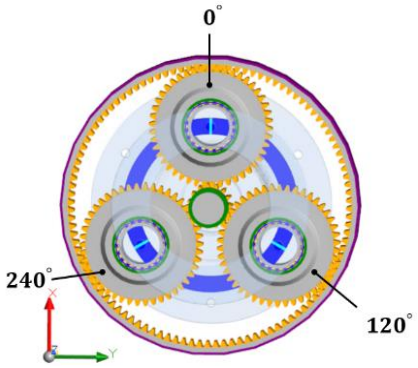

(a) 1st stage planetary gear phase angle

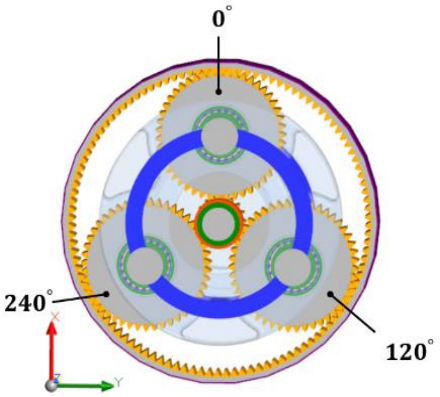

(b) 2nd stage planetary gear phase angle

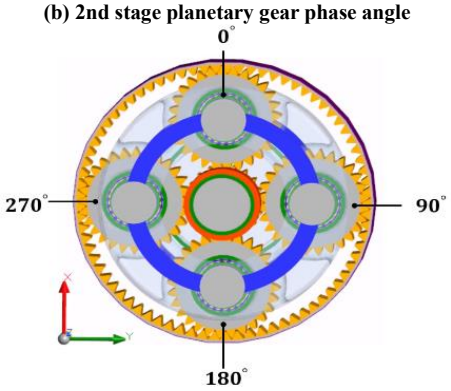

(c) 3rd stage planetary gear phase angle

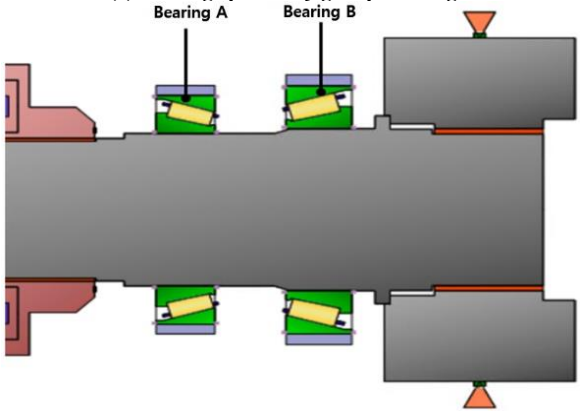

(d) Output Bearing

Fig. 17 Displacement measurement positions on planetary gears and output bearings

Table 8. Speed and frequency

Stage		Number of teeth	Rotational speed (rpm)	Frequency (Hz)
1st	Sun	16	150.9874	40.2613
	Planet	47	44.873	
	Ring	110	0	
2nd	Sun	16	19.173	5.1128
	Planet	25	9.9334	
	Ring	68	0	
3rd	Sun	20	3.652	1.2173
	Planet	23	2.4539	
	Ring	68	0	

Table 9. Acceptable levels of displacement at the gear stage

Stage	Pitch line speed (m/s)	Class	Reference speed (Hz)	Acceptable levels (μm)
1st	0.2213	A	40.2613	67
2nd	0.0562	A	5.1128	86
3rd	0.0172	A	1.2173	400

Table 10. Response analysis results of the 1st-stage planetary gear

	Displacement of 1st-stage planetary gear (μm)		
Planetary gear position	**0°**	**120°**	**240°**
X Direction	50.336	35.784	21.511
Y Direction	14.599	22.348	20.382
Z Direction	42.877	31.387	36.622

Table 11. Response analysis results of the 2nd-stage planetary gear

	Displacement of 2nd-stage planetary gear (μm)		
	0°	**120°**	**240°**
X Direction	14.926	15.395	10.050
Y Direction	11.998	10.754	16.723
Z Direction	11.616	9.315	7.005

Table 12. Response analysis results of the 3rd-stage planetary gear

	Displacement of 3rd-stage planetary gear (μm)			
	0°	**90°**	**180°**	**270°**
X Direction	11.790	12.866	11.791	12.866
Y Direction	12.791	11.719	12.789	11.720
Z Direction	3.919	4.032	4.266	4.1533

Table 13. Response analysis results of the bearing output shaft

	Displacement of 1st-stage planetary gear (μm)	
	Bearing A	**Bearing B**
X Direction	7.844	4.948
Y Direction	6.467	5.296
Z Direction	4.018	3.977

5. Conclusion

This study examined the vibration characteristics of the blade adjustment gear train for an 8MW offshore wind turbine, yielding the following conclusions:

- A method was proposed for analyzing the vibrations of the blade adjustment gear train by combining the rotational vibration model of the planetary gear train with finite element models of the housing and carriers using the substructuring method.
- By applying 10%, 20%, ⋯, 100% of the largest value among LDD loads, it was observed that both bearing stiffness and primary natural frequency increase with higher LDD loads. Furthermore, the primary natural frequency for the highest load in LDD data was found to be 104.26 Hz, which exceeds the operating speed of 84.87 rpm (5.09 Hz), indicating that vibrations due to LDD load variations do not occur within the operating speed range.
- Analysis of critical speeds for the blade adjustment gear train showed that critical speeds related to mass unbalance, gear mesh frequency, and bearing defects (FTF, BS, OR, IR) do not occur within the operating speed range (84.87 rpm).
- To perform a safety assessment of the vibration displacement of the wind turbine blade adjustment gear train, the AGMA 6000-B96 standard was utilized to select an acceptable displacement, and the displacement occurring under extreme load conditions was compared with the acceptable displacement. The response analysis results for the planetary gears and output shaft bearings at the 1st, 2nd, and 3rd stages all met the acceptable levels. This study demonstrates that vibration problems in complex gear systems can be predicted in the simulation phase. This can contribute to a dramatic reduction in development costs and time by enabling the discovery and correction of potential design flaws before manufacturing expensive prototypes or conducting real-world tests.

The study focused on theoretical analysis; however, future research aims to construct an experimental setup, like vibration sensors, with actual experiments or modal tests to compare the characteristics of the experimental results with the theoretical predictions. Through this, we hope to validate the theory and explore its practical applications in more detail.

Acknowledgments

This paper presents results of research conducted with support from the “Core Technology Development Project for Renewable Energy,” funded by the Korea Institute of Energy Technology Evaluation and Planning (KETEP) under the Ministry of Trade, Industry and Energy (No. 20213030020020).

References

[1] J.W. David, and L.D. Mitchell, “Linear Dynamic Coupling in Geared Rotor System,” *Journal of Vibration, Acoustics, Stress, and Reliability in Design*, vol. 108, no. 2, pp. 171-176, 1986. [CrossRef] [Google Scholar] [Publisher Link]

[2] L.D. Mitchell, and J.W. David, “Proposed Solution Methodology for the Dynamically Coupled Nonlinear Geared Rotor Mechanics Equations,” *Journal of Vibration, Acoustics, Stress, and Reliability in Design*, vol. 107, no. 1, pp. 112-116, 1985. [CrossRef] [Google Scholar] [Publisher Link]

[3] Takuzo Iwatsubo, Shirou Arii, and Ryoji Kawai, “Coupled Lateral-Torsional Vibration of Rotor System Trained by Gears : Part 1. Analysis by Transfer Matrix Method,” *Bulletin of Japanese Society of Mechanical Engineers*, vol. 27, no. 224, pp. 271-277, 1984. [CrossRef] [Google Scholar] [Publisher Link]

[4] Hiroshi Iida et al., “Coupled Torsional-Flexural Vibration of a Shaft in a Geared System of Rotors : 1st Report,” *Bulletin of the JSME*, vol. 23, no. 186, pp. 2111-2117, 1980. [CrossRef] [Google Scholar] [Publisher Link]

[5] Hiroshi Iida, Akiyoshi Tamura, and Hiroshi Yamamoto, “Dynamic Characteristics of a Gear Train System with Softly Supported Shafts,” *Bulletin of JSME*, vol. 29, no. 252, pp. 1811-1816, 1986. [CrossRef] [Google Scholar] [Publisher Link]

[6] P. Schwibinger, and R. Nordmann, “The Influence of Torsional-Lateral Coupling on the Stability Behavior of Geared Rotor Systems,” *Journal of Engineering for Gas Turbines and Power*, vol. 110, no. 4, pp. 563-571, 1988. [CrossRef] [Google Scholar] [Publisher Link]

[7] A. Kahraman et al., “Dynamic Analysis of Geared Rotors by Finite Elements,” *Journal of Mechanical Design*, vol. 114, no. 3, pp. 507-514, 1992. [CrossRef] [Google Scholar] [Publisher Link]

[8] F.K. Choy et al., “Vibration Signature and Modal Analysis of Multi-stage Gear Transmission,” *Journal of the Franklin Institute*, vol. 328, no. 2-3, pp. 281-298, 1991. [CrossRef] [Google Scholar] [Publisher Link]

[9] F.K. Choy et al., “Modal Simulation of Gear Box Vibration with Experimental Correlation,” *Journal of Propulsion and Power*, vol. 9, no. 2, pp. 301-306, 1993. [CrossRef] [Google Scholar] [Publisher Link]

[10] M. A. Prohl, "General Method for Calculating Critical Speeds of Flexible Rotors," *Journal of Applied Mechanics*, vol. 12, no. 3, pp. A142-A148, 1945. [CrossRef] [Google Scholar] [Publisher Link]

[11] J.W. Lund, "Stability and Damped Critical Speeds of a Flexible Rotor in Fluid-Film Bearings," *Journal of Manufacturing Science and Engineering*, vol. 96, no. 2, pp. 509-517, 1974. [CrossRef] [Google Scholar] [Publisher Link]

[12] P.N. Bansal, and R.G. Kirk, "Stability and Damped Critical Speeds of Rotor-Bearing Systems," *Journal of Manufacturing Science and Engineering*, vol. 97, no. 4, pp. 1325-1332, 1975. [CrossRef] [Google Scholar] [Publisher Link]

[13] Mengyan Nie, and Ling Wang, "Review of Condition Monitoring and Fault Diagnosis Technologies for Wind Turbine Gearbox," *Procedia CIRP*, vol. 11, pp. 287-290, 2013. [CrossRef] [Google Scholar] [Publisher Link]

[14] K. Smolders et al., "Reliability Analysis and Prediction of Wind Turbine Gearboxes," *European Wind Energy Conference and Exhibition*, vol. 4, pp. 2660-2670, 2010. [CrossRef] [Google Scholar] [Publisher Link]

[15] A. Kahraman, "Planetary Gear Train Dynamics," *Journal of Mechanical Design*, vol. 116, no. 3, pp. 713-720, 1994. [CrossRef] [Google Scholar] [Publisher Link]

[16] A. Kahraman, "Natural Modes of Planetary Gear Trains," *Journal of Sound and Vibration*, vol. 173, no. 1, pp. 125-130, 1994. [CrossRef] [Google Scholar] [Publisher Link]

[17] Robert G. Parker, Vinayak Agashe, and Sandeep M. Vijayakar, "Dynamic Response of a Planetary Gear System using a Finite Element/Contact Mechanics Model," *Journal of Mechanical Design Design*, vol. 122, no. 3, pp. 304-310, 2000. [CrossRef] [Google Scholar] [Publisher Link]

[18] Tedric A. Harris, *Rolling Bearing Analysis*, Wiley, pp. 1-1086, 2001. [Google Scholar] [Publisher Link]

[19] Pascal Guay, and Ahmed Frikha, "Ball Bearing Stiffness. A New Approach Offering Analytical Expressions," *Proceedings of 16th European Space Mechanisms and Tribology Symposium*, Bilbao, 2015. [Google Scholar]

[20] Pierre Tchakoua et al., "Wind Turbine Condition Monitoring: State-of-the-Art Review, New Trends, and Future Challenges, New Trends, and Future Challenges," *Energies*, vol. 7, no. 4, pp. 2595-2630, 2014. [CrossRef] [Google Scholar] [Publisher Link]